J. Fluid Mech. (1993), *vol.* 247, *pp.* 1–16

On the nonlinear development of the most unstable Görtler vortex mode

By JAMES P. DENIER AND PHILIP HALL
Department of Mathematics, University of Manchester, Manchester M13 9PL, UK

(Received 24 January 1992 and in revised form 29 July 1992)

The nonlinear development of the most unstable Görtler vortex mode in boundary-layer flows over curved walls is investigated. The most unstable Görtler mode is confined to a viscous wall layer of thickness $O(G^{-\frac{1}{5}})$ and has spanwise wavelength $O(G^{-\frac{1}{5}})$; it is, of course, most relevant to flow situations where the Görtler number $G \gg 1$. The nonlinear equations governing the evolution of this mode over an $O(G^{-\frac{3}{5}})$ streamwise lengthscale are derived and are found to be of a fully non-parallel nature. The solution of these equations is achieved by making use of the numerical scheme used by Hall (1988) for the numerical solution of the nonlinear Görtler equations valid for $O(1)$ Görtler numbers. Thus, the spanwise dependence of the flow is described by a Fourier expansion whereas the streamwise and normal variations of the flow are dealt with by employing a suitable finite-difference discretization of the governing equations. Our calculations demonstrate that, given a suitable initial disturbance, after a brief interval of decay, the energy in all the higher harmonics grows until a singularity is encountered at some downstream position. The structure of the flow field as this singularity is approached suggests that the singularity is responsible for the vortices, which are initially confined to the thin viscous wall layer, moving away from the wall and into the core of the boundary layer.

1. Introduction

Our concern is with the effect of nonlinearity on the growth of the most unstable Görtler mode in the high Reynolds number flow over a wall of variable curvature. The most unstable Görtler mode was recently identified by Denier, Hall & Seddougui (1990, 1991) who, in the context of the receptivity problem for Görtler vortices, re-examined the linear Görtler equations in the limit of large Görtler number, G. Denier *et al.* (1990, 1991 hereafter referred to as DHS), investigated both the inviscid Görtler vortex modes of $O(1)$ wavenumber and the right-hand branch modes of $O(G^{\frac{1}{4}})$ wavenumber previously considered by Hall (1982*a*), and were able to demonstrate the existence of a most unstable Görtler mode. This mode was found to lie in the wavenumber regime $O(G^{\frac{1}{5}})$ with a spatial growth rate $O(G^{\frac{2}{5}})$ (see figure 1) and was found to be confined to a thin, $O(G^{-\frac{1}{5}})$, viscous layer located at the material boundary. This should be compared with the inviscid and right-hand-branch Görtler modes which have growth rates $O(G^{\frac{1}{2}})$. Note that it is readily shown that for the temporal evolution of Görtler vortices the growth rates are of $O(G^{\frac{1}{2}})$ over the whole wavenumber spectrum; in fact the temporal evolution of the Görtler vortex modes is of no practical interest since in situations where Görtler vortices are found to occur experimentally their initial development is apparently independent of time. An independent investigation of the growth rates of Görtler vortices at high Görtler

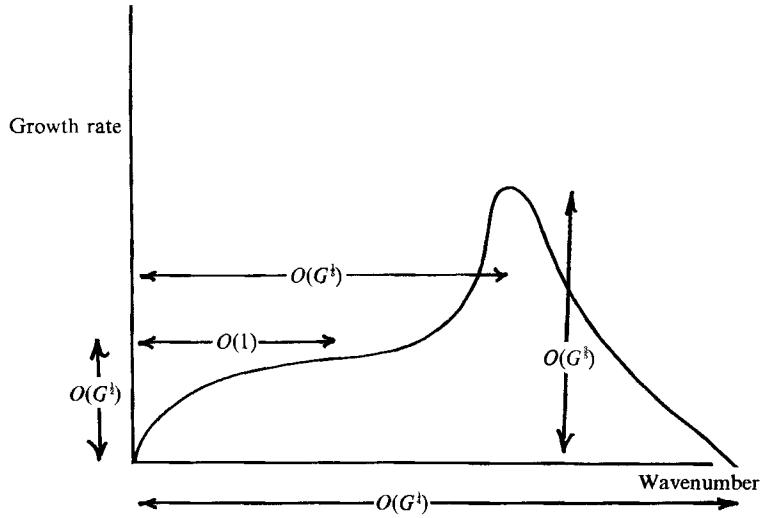

FIGURE 1. A schematic representation of the growth rate versus wavenumber in the large Görtler number limit. The regions corresponding to the inviscid, most unstable and right-hand branch Görtler modes, respectively, are marked.

numbers is given by Timoshin (1991); the conclusions of Timoshin are consistent with DHS.

Previous investigations into the nonlinear evolution of Görtler vortices in spatially growing flows are limited to the work of Hall (1988), in which the fully nonlinear Görtler governing equations were solved numerically for both $O(1)$ wavenumber and Görtler number, and that of Hall & Lakin (1988), in which a fully nonlinear mean flow/first harmonic theory is developed for the right-hand branch Görtler modes. (See also Aihara 1976 who derived a nonlinear differential equation to determine the evolution of Görtler vortices; this calculation, however, ignores non-parallel effects present due to boundary-layer growth and employs other approximations which cannot be justified.) However, for a discussion of Görtler vortices in unsteady boundary layers see for example Sabry & Liu (1991) for impulsively started flows and Hall (1984) for time-periodic flows. Note in addition that Sabry & Liu infer a connection between the growth of vortices in impulsively started flows and Blasius flow. The results of Hall (1988), which are applicable to $O(1)$ wavenumbers and Görtler numbers for which a full numerical treatment of the nonlinear equations governing the vortex evolution is required, demonstrated that as the vortex evolves downstream the energy of the flow becomes concentrated in the mean flow correction and fundamental harmonic. These results, coupled with the fact that the effect of nonlinearity in this problem is to stabilize the flow, suggest that the far downstream structure of the velocity field, in the absence of any unstable secondary modes which might exist (see also §4), is governed by a first harmonic/mean flow theory. Motivated by these results, together with the earlier weakly nonlinear theory of Hall (1982*b*), Hall & Lakin (1988) (also see related work by Benney & Chow 1989) subsequently developed a first harmonic/mean flow theory for short-wavelength large-amplitude Görtler vortices. (We note that the small-wavelength approximation inherent in this theory is not physically unrealistic since for a growing boundary layer the effective wavenumber of the Görtler vortices increases in the downstream direction.) This theory then demonstrates that the mean flow adjusts due to the presence of the vortex state so as to render the large-amplitude vortices neutrally

stable. The mean flow is then driven by the vortex velocity field and its form is completely altered from that which exists in the absence of the vortex motion. Subsequently Hall & Seddougui (1990) showed that the large-amplitude vortex states found by Hall & Lakin (1988) are unstable to wavy vortex modes trapped in the shear layers bounding the region of vortex activity.

The above results, however, are not directly applicable to situations where the Görtler number is large and the wavenumber is not close to its neutral value. Here we would expect, on the basis of the linear receptivity theory of DHS, the most unstable linear Görtler mode to be excited by, for example, small localized surface imperfections. One such area where this scenario would be applicable is the flow over turbine blades where, due to the large Reynolds numbers encountered in such situations together with an appreciable curvature, we would anticipate large Görtler numbers and thus the possible excitation of the most unstable Görtler mode through the presence of small surface defects. For these reasons a study of the nonlinear evolution of the most unstable Görtler modes is both warranted and is of real practical importance.

The outline of the rest of the paper is as follows. In §2 we derive the nonlinear equations governing the downstream evolution of the most unstable Görtler vortex mode. A brief discussion of the numerical scheme employed to solve these equations is given. In §3 we present the results of our numerical calculations along with a discussion of these results. Finally in §4 we draw some conclusions.

2. Formulation of the governing equations

Consider the flow of a viscous incompressible fluid, of density ρ and kinematic viscosity ν, over a wall of variable curvature $a^{-1}\chi(x/L)$. Here a and L are the typical lengthscales associated with the radius of curvature of the wall and the downstream development of the flow, respectively. Denoting by U_∞ the free-stream speed, sufficiently far from the wall, we define the usual Reynolds number Re by

$$Re = U_\infty L/\nu, \tag{2.1}$$

and restrict our attention to the limit $Re \to \infty$ with the Görtler number, G, defined by

$$G = (2L/a)Re^{\frac{1}{2}}, \tag{2.2}$$

held fixed. Let (x, y, z) denote the usual Cartesian coordinates, non-dimensionalized with respect to L, $LRe^{-\frac{1}{2}}$, $LRe^{-\frac{1}{2}}$ respectively. The corresponding velocity field is taken to be

$$\boldsymbol{u} = U_\infty(\bar{u}+u, Re^{-\frac{1}{2}}(\bar{v}+v), Re^{-\frac{1}{2}}w), \tag{2.3}$$

where we will assume that $(\bar{u}(x,y), \bar{v}(x,y), 0)$ corresponds to the Blasius boundary layer, and that (u, v, w) and the corresponding pressure perturbation p are functions of (x, y, z). By substituting the above relations into the Navier–Stokes and continuity equations we find the governing equations for u, v, w and p, correct to $O(Re^{-\frac{1}{2}})$, to be given by

$$\left.\begin{aligned} u_x + v_y + w_z &= 0, \\ u_{yy} + u_{zz} - v\bar{u}_y &= \bar{u}u_x + \bar{u}_x u + \bar{v}u_y + Q_1, \\ v_{yy} + v_{zz} - G\chi\bar{u}u - p_y &= \bar{u}v_x + \bar{v}_x u + \bar{v}v_y + \bar{v}_y v + Q_2, \\ w_{yy} + w_{zz} - p_z &= \bar{u}w_x + \bar{v}w_y + Q_3. \end{aligned}\right\} \tag{2.4}$$

Here the nonlinear functions Q_1, Q_2, Q_3 are given by

$$Q_1 = uu_x + vu_y + wu_z, \quad Q_2 = uv_x + vv_y + wv_z + \tfrac{1}{2}G\chi u^2, \quad Q_3 = uw_x + vw_y + ww_z. \tag{2.5}$$

Note that we have implicitly assumed above that Görtler vortices develop spatially so that time derivatives of the velocity field have been neglected. We have made this assumption because the fastest growing mode of DHS is intrinsically a spatial rather than a temporal mode and because there are no experiments which suggest the importance of unsteady effects in the initiation of Görtler vortices. Thus we are in effect assuming that the Görtler mechanism in the wavenumber regime under consideration is a convective instability mechanism. However recently Ruban (1990) has argued that at low vortex wavenumbers the Görtler mechanism is an absolute instability. The latter result is not consistent with experimental observations and is contradicted by recent work by Choudhary & Hall (1992). By setting the nonlinear terms Q_1, Q_2, Q_3 equal to zero in (2.4) we recover the linearized equations of Hall (1983). In the limit of large spanwise wavenumber, $\partial/\partial z \gg 1$, Hall (1982*a*) demonstrated that in this regime the right-hand branch of the neutral curve scales as $G = O(k^4)$, where $k \gg 1$ is the spanwise wavenumber.

For $O(1)$ values of the Görtler number the fully nonlinear system (2.4) has been solved numerically by Hall (1988). However, in situations in which the Görtler number is large, the results of this work would be of limited relevance since we would expect that in this case the most unstable linear Görtler mode would soon dominate the flow field. In fact, the receptivity problem for the most unstable mode has been considered by DHS who demonstrated that the coupling coefficient between a surface perturbation and the induced velocity field is an $O(1)$ quantity and as such we would expect these modes to be generated by, for example, isolated roughness elements on the surface.

To consider the nonlinear development of the most unstable Görtler mode we define new variables

$$Y = G^{\frac{1}{5}}y, \quad Z = G^{\frac{1}{5}}z, \quad X = G^{\frac{2}{5}}(x - x^*), \tag{2.6}$$

and expand the velocity field and pressure in the form

$$(u, v, w, p) = G^{\frac{1}{5}}(G^{-\frac{2}{5}}U, V, W, G^{\frac{1}{5}}P) + \ldots. \tag{2.7}$$

Here, the scaling in X anticipates the result from DHS that the downstream growth rate of the most unstable Görtler mode is $O(G^{\frac{2}{5}})$. The governing equations (2.4) then become, to leading order in powers of $G^{-\frac{1}{5}}$,

$$\begin{aligned} U_X + V_Y + W_Z &= 0, \\ U_{YY} + U_{ZZ} - \mu(x^*)\, V &= \mu Y U_X + U U_X + V U_Y + W U_Z, \\ V_{YY} + V_{ZZ} - \chi(x^*)\,\mu Y U - P_Y &= \mu Y V_X + U V_X + V V_Y + W V_Z + \tfrac{1}{2}\chi(x^*)\, U^2, \\ W_{YY} + W_{ZZ} - P_Z &= \mu Y W_X + U W_X + V W_Y + W W_Z, \end{aligned}$$

where we have made use of the fact that $\bar{u} \sim \mu(x^*)\, y + \ldots$ as $y \to 0$. With a suitable rescaling we can remove the constant coefficients in the above system, and hence, without loss of generality, we will assume $\mu = \chi = 1$ in the above system. The governing equations are then

$$U_X + V_Y + W_Z = 0, \tag{2.8a}$$

$$U_{YY} + U_{ZZ} - V = Y U_X + U U_X + V U_Y + W U_Z, \tag{2.8b}$$

$$V_{YY} + V_{ZZ} - Y U - P_Y = Y V_X + U V_X + V V_Y + W V_Z + \tfrac{1}{2}U^2, \tag{2.8c}$$

$$W_{YY} + W_{ZZ} - P_Z = Y W_X + U W_X + V W_Y + W W_Z. \tag{2.8d}$$

The boundary conditions appropriate to (2.8) are found to be

$$U = V = W = 0, \quad Y = 0, \qquad U \to A(X), \quad Y \to \infty, \tag{2.9}$$

where the displacement function A is independent of Z (ensuring that the nonlinear vortex state is confined to the wall layer). We note here that A is completely determined by the wall-layer solution. To complete the description of the flow regime we require a region where $y = O(1)$ in which the mean flow adjusts to its free-stream value. However, that region is passive so we shall not consider it here. The nonlinear system (2.8), (2.9) is the nonlinear generalization of DHS and was previously written down, but not solved, by Timoshin (1991).

In order to reduce the system (2.8) to a form suitable for computational purposes we eliminate W and P from the linear terms in (2.8c, d) to give

$$\left\{\left(\frac{\partial^2}{\partial Y^2}+\frac{\partial^2}{\partial Z^2}\right)-Y\frac{\partial}{\partial X}\right\}\left(\frac{\partial^2}{\partial Y^2}+\frac{\partial^2}{\partial Z^2}\right)V-YU_{ZZ}=-N_{1XY}+N_{2ZZ}-N_{3YZ}, \tag{2.10}$$

where

$$N_1=UU_X+VU_Y+WU_Z,\quad N_2=UV_X+VV_Y+WV_Z+\tfrac{1}{2}U^2,\quad N_3=UW_X+VW_Y+WW_Z. \tag{2.11}$$

The numerical procedure employed in the solution of (2.8a, b) and (2.10) subject to the boundary conditions (2.9) is based on that used by Hall (1988) in the solution of the nonlinear Görtler equations at $O(1)$ Görtler numbers, and for this reason we give only the salient details of the scheme here.

Anticipating the well-known result that nonlinear interactions in the Görtler and Taylor problems do not generate a mean flow component in the spanwise direction we write

$$(U,V)=(U_0,V_0)+\sum_{n=1}^{\infty}(U_n,V_n)\cos nkz,\quad W=\sum_{n=1}^{\infty}W_n\sin nkz, \tag{2.12}$$

where, without loss of generality, we have chosen the origin in the spanwise direction such that U and V are even in Z whilst W is odd in Z. Substituting the expansions (2.12) into (2.8a, b) and (2.10) and equating like Fourier components gives, for the mean flow correction,

$$U_{0YY}-V_0=YU_{0X}+U_0U_{0X}+V_0U_{0Y}+F_0, \tag{2.13}$$

where

$$F_0=\frac{1}{2}\sum_{m=1}^{\infty}\{V_mU_{mY}-U_mV_{mY}-2kmU_mW_m\},$$

whilst V_0 is determined from

$$\frac{\partial U_0}{\partial X}+\frac{\partial V_0}{\partial Y}=0. \tag{2.14}$$

From a computational standpoint we must necessarily truncate the infinite sums occurring in (2.12) at some suitably large value of the upper limit. Therefore we will formally replace the upper limit in (2.12) by N.

The governing equation for the higher-harmonics terms is then given by

$$\begin{aligned}U_{nyy}-n^2k^2U_n-(1+U_{0Y})V_n-(Y+U_0)U_{nX}&=F_n\\
&=\sum_{\substack{m=1\\ n\neq 1}}^{N-1}V_{n-m}U_{mY}-U_{n-m}V_{mY}-mkW_{n-m}U_m-mkU_{n-m}W_m\\
&\quad+\sum_{\substack{m=1\\ n\neq N}}^{N-n}V_{n+m}U_{mY}-U_{n+m}V_{mY}-mkW_{n+m}U_m-mkU_{n+m}W_m\\
&\quad+\sum_{\substack{m=n+1\\ n\neq N}}^{N}V_{m-n}U_{mY}-U_{m-n}V_{mY}-mkW_{m-n}U_m-mkU_{m-n}W_m,\end{aligned} \tag{2.15}$$

where we have made use of the continuity equation to eliminate the X-derivatives on U_m from the nonlinear terms on the right-hand side of (2.15). A similar equation governing the evolution of the components V_n can be obtained from (2.10) which, for brevity, is not presented here.

We now proceed with a brief description of the scheme used to solve (2.13), (2.15) together with the corresponding equation for the V_n. Suppose then that U_0, V_0 and U_n, V_n, W_n, for $n = 1, 2, \ldots, N$ are known at some particular X-station, X_0 say. The mean flow equation (2.13) is discretized using finite differences in the X- and Y-directions according to

$$\left\{\frac{U_0^{n+1m+1}-2U_0^{nm+1}+U_0^{n-1m+1}}{h^2}\right\}-nh\left\{\frac{U_0^{nm+1}-U_0^{nm}}{\epsilon}\right\}-V_0^{nm}$$

$$=U_0^{nk+1}\left\{\frac{U_0^{nk+1}-U_0^{nk}}{\epsilon}\right\}+V_0^{nk+1}\left\{\frac{U_0^{n+1k+1}-U_0^{n-1k+1}}{2h}\right\}+F_0^{nk+1}. \quad (2.16)$$

Here the indices m and n refer to the grid point $X = X_0+m\epsilon$, $Y = nh$. Initially the nonlinear terms on the right-hand side of (2.16) are evaluated with $k = m-1$ which yields a tridiagonal system for U_0 at $X = X_0+(m+1)\epsilon$. Similarly the finite-difference discretization of (2.15) can be used to give U_m $(m = 1, \ldots, N)$ at $X = X_0+(m+1)\epsilon$ as can the corresponding equation for V_m, but now by solving a pentadiagonal system. The nonlinear terms can now be expressed in terms of the velocity field evaluated at $X = X_0+(m+1)\epsilon$ and the equations are again solved for the flow quantities at $X = X_0+(m+1)\epsilon$, repeating the iteration procedure until the changes in U_0^{m+1} etc. are sufficiently small. In this way (2.16) and the corresponding equations for U_m, V_m are solved for $k = m$ by iterating on the nonlinear terms on the right-hand sides. This scheme can then be used to march the solution downstream from some initial position given some suitable form of initial perturbation to the velocity field.

3. Results and discussion

We now describe the results obtained from the numerical scheme outlined above. All results presented are for the choice of wavenumber $k = 0.476$ which corresponds to the critical wavenumber of the most unstable Görtler mode identified by DHS; some discussion on the form of the solutions for different values of the wavenumber will be given. The basic state was perturbed at $X = 1$ by imposing the disturbance

$$U_1(Y) = \tfrac{1}{8}AY^6\exp(-\tfrac{1}{2}Y^2), \quad V_1(Y) = 0, \quad (3.1)$$

and integrating the linearized equations to $X = 101$. Here A is a measure of the disturbance amplitude. At this stage the disturbance has attained its maximum growth rate according to linear theory (see DHS). The linear velocity field was then given an amplitude equal to the maximum X-velocity component whilst all higher harmonics were set equal to zero. The nonlinear equations were then integrated for $X > 101$.

We note that the precise form of the initial perturbation (3.1) is of little importance in the linear stage of the evolution of the most unstable mode. This can be seen by considering the linearized version of the governing equations; a comparison between the present work and the eigenvalue problem of DHS (see their equation (5.14)) shows that the linearized governing equations, subject to the initial condition (3.1),

constitute an initial-value problem corresponding to the given spanwise wavenumber. Thus, given any reasonable initial condition (i.e. one which satisfies all the boundary conditions on the disturbance velocity field) the solution of the linearized equations will evolve downstream into the characteristic shape of the eigenfunction of DHS (in fact, the downstream form of the velocity field will be a constant multiple of this eigenfunction) and the linear growth rate will approach the value found from the eigenvalue problem; for the results presented here this corresponds to $k = 0.476$, $\beta = 0.312$ (here β is the linear growth rate). This should be compared with the corresponding results of Hall (1983), for the evolution of vortices with $O(1)$ Görtler number, where the growth rate and the structure of the linear modes exhibit a sensitive dependence on both the form of the initial disturbance and the position at which the initial disturbance is imposed. This difference is readily explained by the fact that the most unstable mode of DHS evolves in what is essentially a parallel manner (due in turn to the small x-scale over which these modes develop) whereas the linear modes of Hall (1983) exhibit an inherent non-parallel structure (due to the $O(1)$ x-scale over which these modes develop). Having demonstrated that any reasonable initial conditions will evolve rapidly into the fastest growing mode of DHS we could equally well start the nonlinear calculation at $X = 101$ with the eigenfunction of the fastest growing mode. The results obtained by starting the nonlinear calculation in this way are indistinguishable from those presented here.

In order to measure the growth of the harmonic components of the flow field we define the energy of the nth harmonic to be

$$E_n = \int_0^\infty \{U_n^2(X,Y) + V_n^2(X,Y) + W_n^2(X,Y)\}\,\mathrm{d}Y, \quad n = 1, 2, \ldots. \tag{3.2}$$

Note that we do not calculate the energy of the mean flow correction as in Hall (1988) since in the present case we have $U_0 \to U_0(X)$ when $Y \to \infty$. The growth rate $\sigma_n(X)$ of the nth mode is then defined as

$$\sigma_n(X) = \frac{1}{E_n(X)} \frac{\mathrm{d}E_n(X)}{\mathrm{d}X}. \tag{3.3}$$

In the absence of the nonlinear terms the growth rate $\sigma_1(X)$ would be twice that calculated by DHS; in the light of the discussion of the previous paragraph $\sigma_1(X) \to 0.624$ as $X \to \infty$ (see figure 2).

With the perturbation to the basic state given by (3.1) the governing equations were solved for the choice of parameters $h = 0.1$, $\epsilon = 0.001$ with $Y_\infty = 100$ (corresponding to 1000 grid points in the normal direction). These values were chosen after significant testing of the code for accuracy and stability. With h fixed the calculations were carried out for various values of ϵ until the results from consecutive runs agreed to within graphical accuracy. The streamwise step size ϵ was then fixed and h was decreased, with Y_∞ fixed, until, again, the results from consecutive calculations had converged, to within graphical accuracy. We then fixed both ϵ and h and varied Y_∞ which resulted in little or no change in the computed flow quantities. It was found that the numerical scheme was stable for $\epsilon = O(h^2)$. In figure 3 we present a comparison between calculations performed for $\epsilon = 0.002$ and $\epsilon = 0.001$ with the normal step length $h = 0.1$ fixed (see figure caption). Up until the stage at which the calculation for $\epsilon = 0.001$ fails the results are identical (note that the results for $\epsilon = 0.002$ have been offset). However, there is a small, yet significant, discrepancy on the position at which the breakdown occurs. We interpret this discrepancy in the

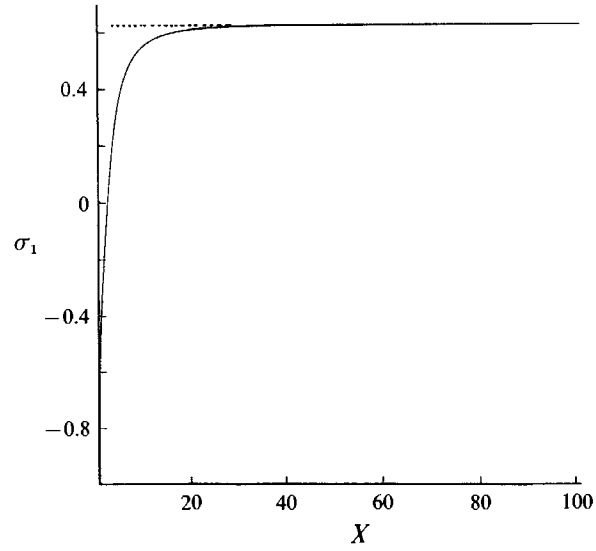

FIGURE 2. The linear growth rate σ_1 versus X for wavenumber $k = 0.476$. Dashed line shows the position of the most unstable mode of DHS.

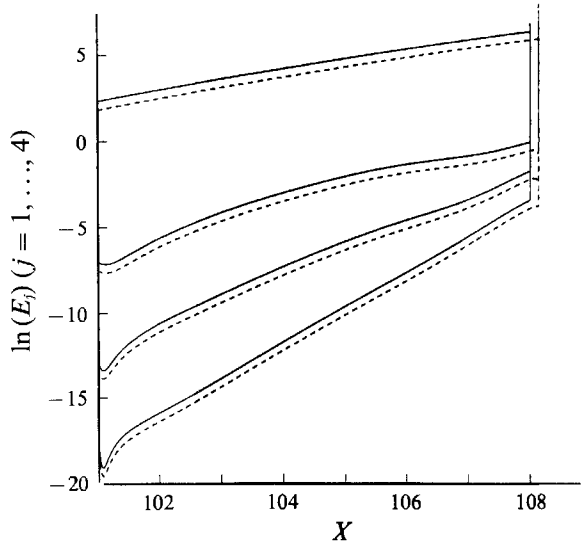

FIGURE 3. Comparison of results obtained for different streamwise step lengths. Solid line $\epsilon = 0.001$, broken line $\epsilon = 0.002$. In order to distinguish the plots for $\epsilon = 0.002$ these have been offset by -0.5. Plotted in $\ln(E_j)$ $(j = 1, \ldots, 4)$ versus X.

breakdown position which occurs for the larger of the two values of ϵ as being due to the numerical scheme essentially 'jumping' over the breakdown position and continuing into a region where, in fact, the numerical code is no longer valid. Various calculations were done for which $N = 4$, 8 and 16 Fourier modes in the spanwise direction were retained; the results presented are for the case $N = 8$ (the results from the calculations for $N = 4$ and 16 show little, if any variations from those obtained for $N = 8$). In figure 4 we present a comparison of the results obtained with $N = 8$ and

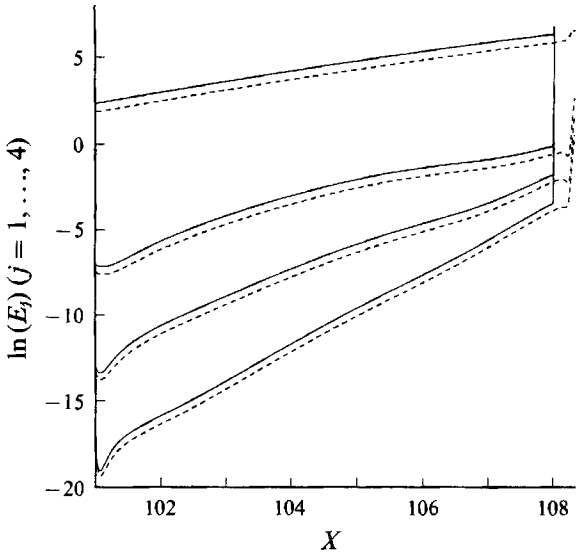

FIGURE 4. Comparison of results obtained by retaining different numbers of Fourier modes. Solid line $N = 8$, dashed line $N = 16$. In order to distinguish the plots for $N = 16$ these have been offset by -0.5. Owing to limitations on available computing time the results for $N = 16$ were obtained for a streamwise step length of $\epsilon = 0.01$.

16 Fourier modes retained in the expansions (2.12). Again the results are identical, to within graphical accuracy for the two cases. (Note that the discrepancy in the breakdown positions for the $N = 8$ and 16 calculations is due to the increased streamwise step length required to make the latter calculation feasible.) The parameter values quoted above were then chosen with two criteria in mind; firstly they were chosen to be suitably small in order to resolve both the normal and streamwise structure of the flow in the later stages of the calculations and secondly they were chosen so as to allow the calculations to be performed in an acceptable amount of time. All results presented were obtained on a Cray Y-MP at the NASA Langley Research Centre.

In figure 5 we present a plot of the energy of the nth harmonic as a function of downstream position X. Here we see that, after an initial interval of decay due to the solution rapidly adjusting from its linear state to a fully nonlinear state in which the mean flow correction is driven by the vortex velocity field, the energy in each mode is a monotonically increasing function of x. This was found to continue until the point where the energy in each harmonic undergoes a period of rapid growth (occurring over a small streamwise interval). However, at this stage of the calculation a point of separation has been encountered beyond which we expect reversed flow. Our numerical scheme is then no longer valid, as it relies on the parabolic nature of the governing equations and as such is not able to deal with the reversed flow in the streamwise direction. Numerous calculations were performed in order to verify this; in particular, increasing the number of modes retained in our expansions from $N = 8$ to $N = 16$. The results from this calculation were found to agree with those for $N = 8$ Fourier modes to within the graphical accuracy of figure 5. Similarly, decreasing the step size in the streamwise direction was found to have little effect on the results of the calculation. All results presented were obtained for the input disturbance amplitude $A = 0.075$. In order to test the effect of varying the amplitude of the initial disturbance velocity field we repeated our calculations for

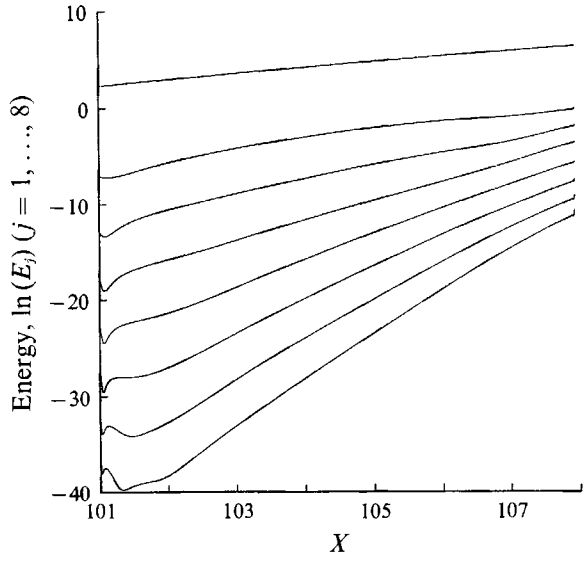

FIGURE 5. Plot of $\ln(E_j)$ $(j = 1, \ldots, 8)$ versus downstream position X.

various values of the amplitude Δ. The results of these calculations demonstrated that varying Δ had no qualitative effect upon the breakdown which is encountered for the case presented, namely $\Delta = 0.075$; decreasing Δ has the effect of delaying the breakdown. For this reason we restrict our attention to the case $\Delta = 0.075$; the results presented can then be considered as typical for the whole range of input amplitudes.

Before proceeding with a discussion of this breakdown we make some comparison of our results with those of Hall (1988). In figure 6 we present a plot of the growth rates σ_n $(n = 1, \ldots, 8)$ as a function of the downstream position X. Here we see that the growth rates, after an initial adjustment stage wherein the flow adjusts in order to accommodate the nonlinear terms, increase with increasing X; in fact the growth rates are ordered such that $\sigma_j > \sigma_{j-1}$ $(j = 2, \ldots, 8)$. However, the growth rate of the first harmonic, σ_1, is decreased from that found in the absence of the nonlinear terms; in this respect nonlinear effects are stabilizing. This should be compared with the results of Hall (1988) who found a similar result in that the growth of the first harmonic is decreased in comparison with that obtained from the linearized system. However, an important distinction arises between the present work and that of Hall (1988) in that for the case of $O(1)$ Görtler numbers and wavenumbers the energy is distributed predominantly in the first harmonic and mean flow correction whereas in the present case no such partition of energy is found.

We now turn our attention to a discussion of the breakdown alluded to above. As noted earlier our numerical scheme was found to break down at some downstream position. This breakdown was characterized by the normal, and subsequently the spanwise, components of the velocity field undergoing a period of rapid growth over a small streamwise interval, typically of the order of 5 streamwise step lengths, whereas the streamwise velocity component shows little, if any, variation over this interval.

In order to determine whether this breakdown was due to a singularity of the governing equations, we repeated our calculations with an increased number of Fourier modes retained. As each higher harmonic is forced by it lower harmonics we

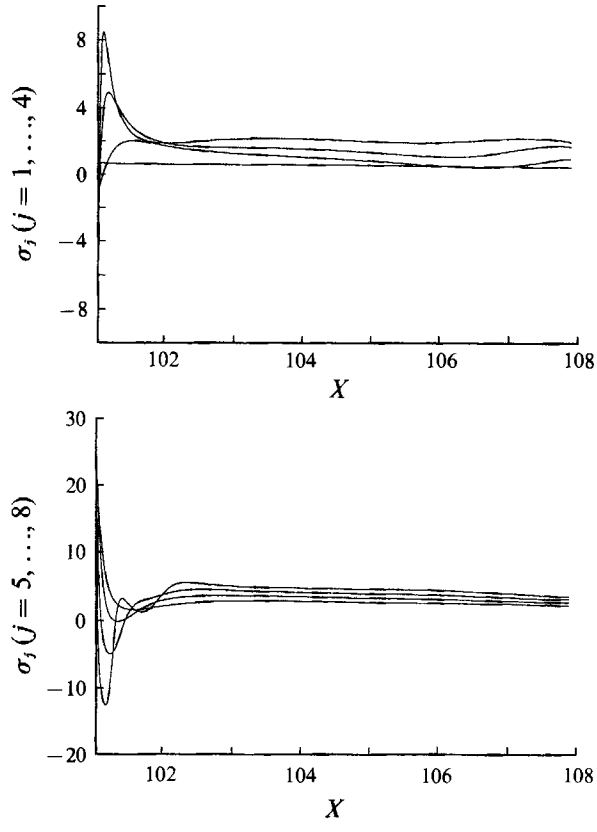

FIGURE 6. The nonlinear growth rates σ_j $(j = 1, \ldots, 8)$ versus X.

would expect that, if such a singularity were encountered, increasing the number of Fourier modes retained in our calculations would have a dramatic effect upon the latter stages of the calculation. However, this was found not to be the case. The inclusion of additional Fourier modes was found to have little effect on the breakdown. For this reason we feel justified in eliminating the possibility of a spanwise localized singularity in the governing equations as being the underlying cause for the breakdown which is encountered.

In the light of the above discussion an alternative mechanism for the breakdown must be found. An obvious candidate immediately presents itself in the form of a singularity due to flow separation. From the work of Hall (1988) we know that flow separation is encountered in the problem of $O(1)$-wavelength Görtler vortices at $O(1)$ Görtler numbers (see also the discussion in Hall & Horseman 1991). As such, flow separation would appear as the likely candidate for the breakdown experienced in the present problem.

In order to test this conjecture we calculated the total skin friction

$$\tau_T(X, Z) = 1 + \sum_{n=0}^{N} U_{nY}(X, 0) \cos knZ, \tag{3.4}$$

at each downstream position on a uniform spanwise grid of 100 points over one half vortex wavelength. Here, we note that the first term on the right-hand side of (3.4)

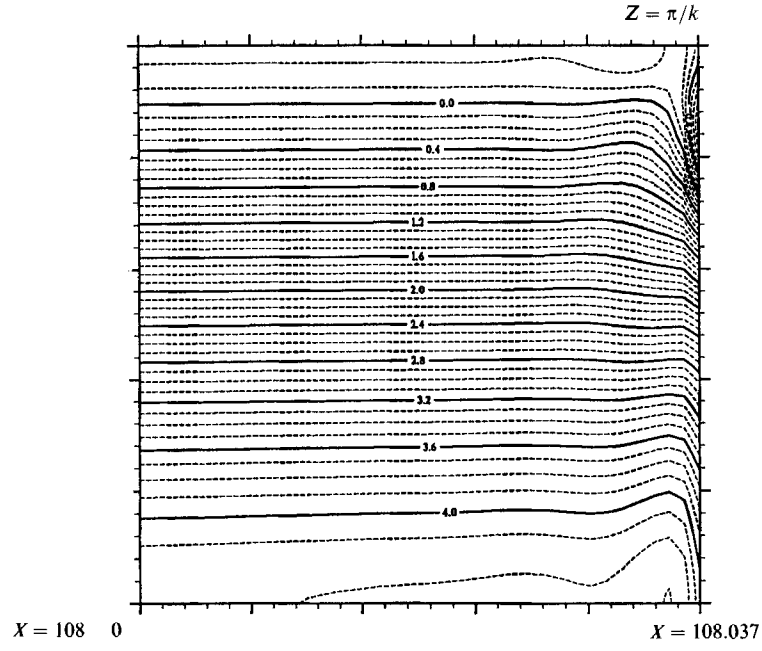

FIGURE 7. Contour plot of the skin friction $(\tau_T - 1)$ in the (X, Z)-plane. Here X is in the interval $(108, 108.037)$ and Z is in the range $(0, \pi/a)$.

arises from the uniform shear, $\bar{u} \sim Y$, in the wall layer (see (2.8)). The point (X^*, Z^*) of flow separation is then defined by

$$\tau_T(X^*, Z^*) = 0.$$

At such a point our finite-difference discretization in the downstream variable X is no longer valid as it does not allow for reversed flow. In figure 7 we present a contour plot of $(\tau_T - 1)$ in the (X, Z)-plane for X in the range $(108, 108.037)$ and Z in the range $(0, \pi/a)$. Here we see that, after an interval of little variation, the total skin friction rapidly decreases until the last downstream location, at which $(\tau_T - 1)$ is negative and separation has occurred. At this point in our calculation the numerical scheme used is no longer valid for the reason given above. We found it impossible to accurately resolve the position at which separation occurs, though not through any deficiency in the code, but because we had reached the limit of our available computing resources. In fact we expect that the finite-difference approach of Cebeci, Khattab & Stewartson (1981) would be capable of tracing out a curve $Z = Z_s(X)$ on which separation occurs. We believe that this separation is only of marginal interest because before it occurs the inflexional velocity profiles in the downstream direction will be massively unstable to Rayleigh waves; therefore we do not pursue it further here.

Not surprisingly, the point of separation is found to occur at the position $Z = \pi/k$, the position at which upwelling occurs. In figure 8 we present a series of contour plots of constant total streamwise velocity

$$U_T(X, Y, Z) = Y + \sum_{n=0}^{N} U_n(X, Y) \cos knZ,$$

at various downstream positions which shows the initial growth of the vortex. In the

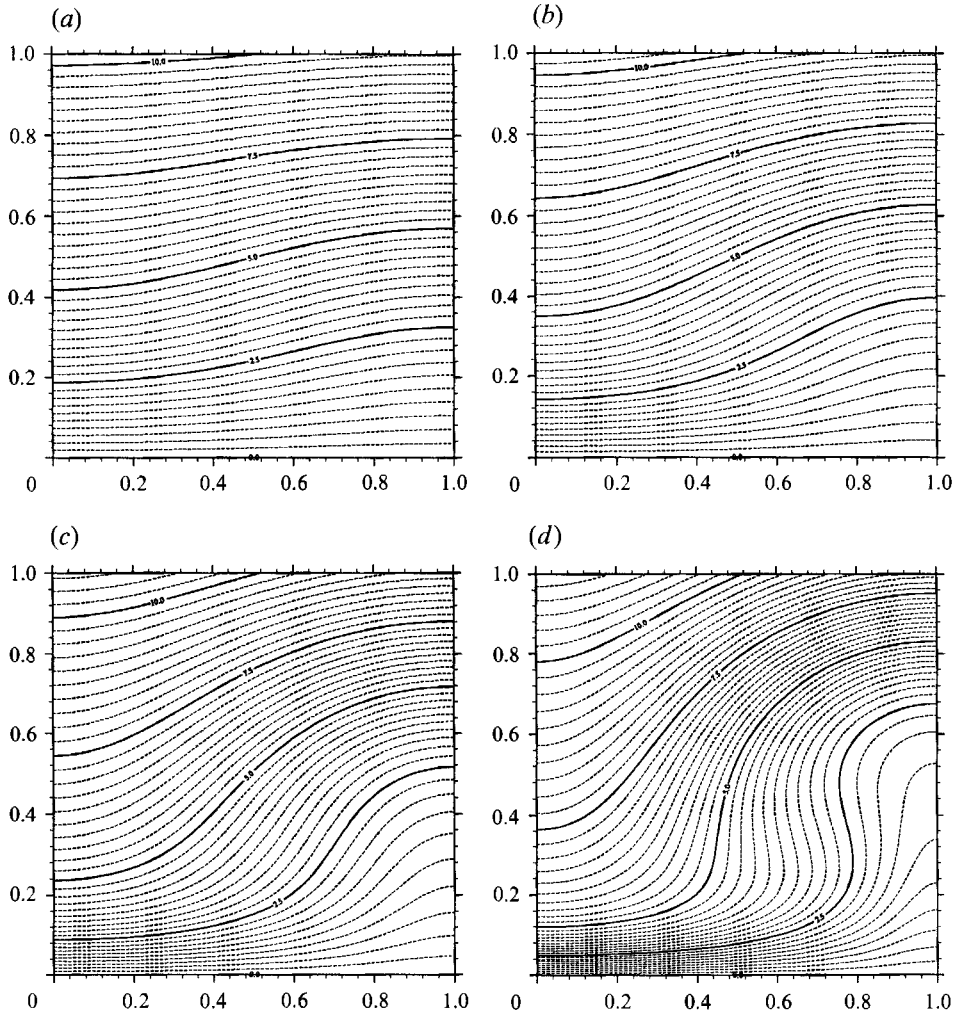

FIGURE 8. Contour plot of the total downstream velocity field at the downstream positions (*a*) $X = 102$, (*b*) $X = 104$, (*c*) $X = 106$, (*d*) $X = 108$.

absence of the nonlinear vortex these plots would appear as a series of equally spaced horizontal lines. The growth of the vortex is then represented by increased curvature of the streamlines of constant streamwise velocity. At $X = 102.0$ (figure 8*a*) the nonlinear vortex has begun to grow until at $X = 108.0$ (figure 8*d*) we see the characteristic shape for Görtler vortices (see Hall & Horseman 1991).

In figure 9(*a–e*) we again present contour plots of the total streamwise velocity at the last five streamwise locations preceding the breakdown of our numerical code. At this stage we see the development of a secondary structure localized about $Z = \pi/a$ in the vicinity of the wall. This structure increasingly distorts the underlying streamlines until at the last point of our calculation (figure 9*e*) the flow is about to become reversed. As noted above we were unable to continue our calculation past the point given for figure 9(*e*), however we would expect that if such a calculation were possible we wound find a small region of reversed flow centred about the point $Z = \pi/a$ which would subsequently increase in size as the calculation were continued downstream.

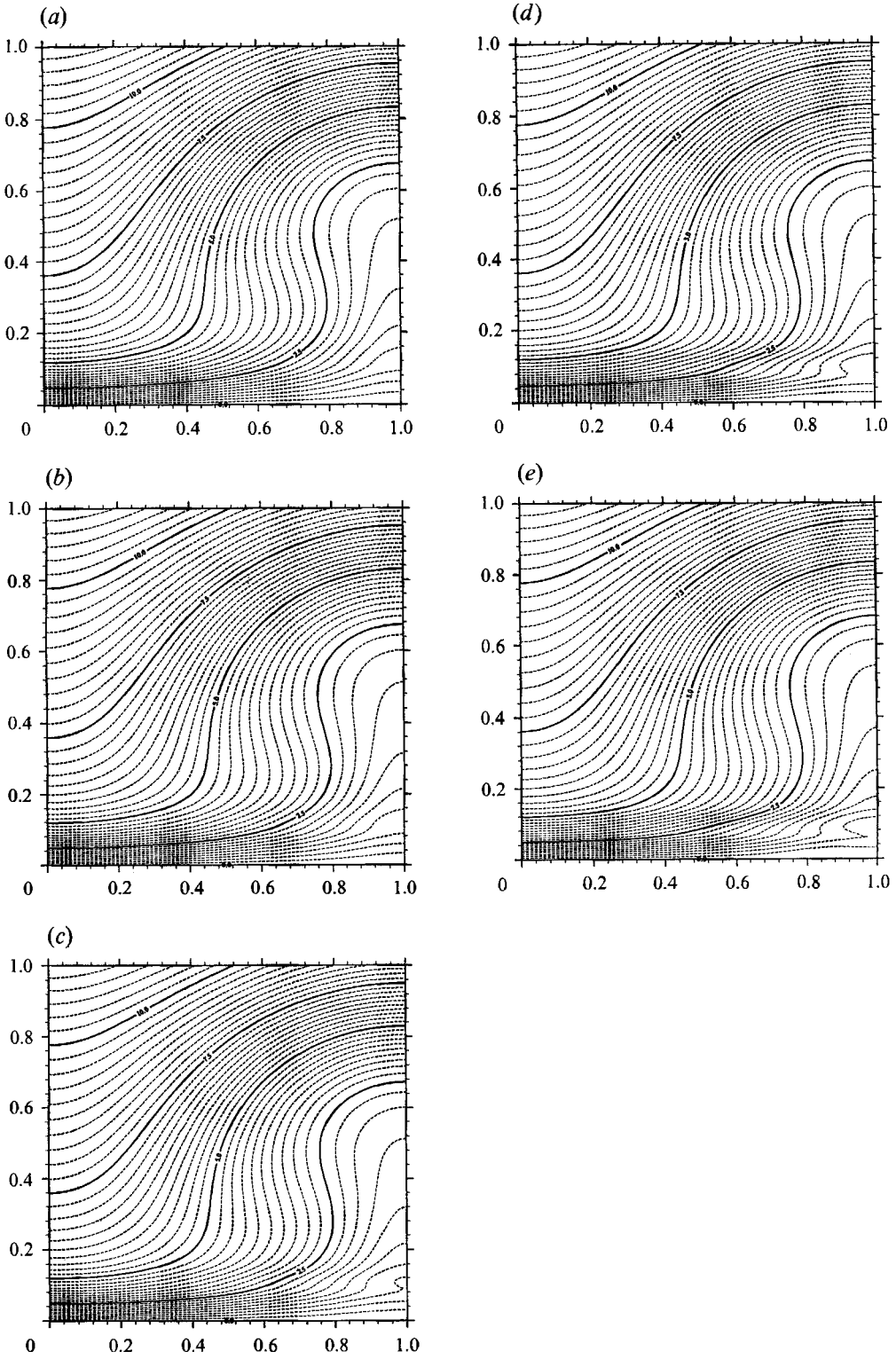

FIGURE 9. Contour plot of the total downstream velocity field in the final stages of the calculation; (*a*) $X = 108.032$, (*b*) $X = 108.033$, (*c*) $X = 108.034$, (*d*) $X = 108.035$, (*e*) $X = 108.036$.

4. Conclusion

We have investigated the spatial nonlinear evolution of the fastest growing Görtler vortex which can occur in a boundary-layer flow . The mode occurs in a quasi-parallel form only at high Görtler numbers so our investigation is particularly relevant to flows where high Reynolds numbers and moderate curvatures are possible. Hence our investigation is, for example, relevant to the flow over turbine blades and also to the flow in jet engine inlets, though compressible effects would certainly be present in the latter case. A crucial feature of the mode is that it occurs adjacent to the wall so that relatively high shear stresses will be induced by its presence.

Our calculations suggest that the nonlinear development of the most unstable Görtler mode results in a reversed flow. Although such a point of separation gives little hope of following the development of these modes downstream past the point of separation we note one important point which arises from our calculations. Recent work on the secondary instability of nonlinear Görtler vortices at $O(1)$ Görtler number by Hall & Horseman (1991) has demonstrated that the fully nonlinear vortex velocity fields obtained numerically by Hall (1988) are highly susceptible to an inviscid Rayleigh instability. This possibility was suggested some years ago by Prandtl (1937). This mode of instability is particularly relevant to flows for which the streamwise velocity field becomes inflexional in both the streamwise *and* spanwise directions. Such a situation arises in the present problem and hence we would expect the flow to be radically altered, due to the linear growth of Rayleigh modes and their subsequent nonlinear evolution, before the point of separation is approached, as is the case for Görtler vortices at $O(1)$ Görtler numbers (see Hall & Horseman 1991 for a discussion). The question is currently under investigation.

Thus we conclude then by noting that our calculations suggest that in relatively highly curved boundary layers, transition will be induced by the Rayleigh instability breakdown of the vortex structures driven by the Görtler instability. It should be noted that alternative instabilities such as Tollmien–Schlichting waves do not have growth rates as large as those of Görtler vortices or Rayleigh waves and are therefore likely to be unimportant in the transition process.

This research was partially supported by the National Aeronautics and Space Administration under NASA Contract No. NAS1-18605 while the authors were in residence at the Institute for Computer Applications in Science and Engineering (ICASE), NASA Langley Research Center, Hampton, VA 23665. The authors also wish to acknowledge SERC for support while this work was in progress.

REFERENCES

AIHARA, Y. 1976 Nonlinear analysis of Görtler vortices. *Phys. Fluids* **19**, 1655.

BENNEY, D. J. & CHOW, K. 1989 Instabilities of waves on a free surface. *Stud. in Appl. Maths* **74**, 227–243.

CEBECI, T., KHATTAB, A. A. & STEWARTSON, K. S. 1981 Three-dimensional boundary layer separation and the ok of accessibility. *J. Fluid Mech.* **107**, 57–82.

CHOUDHARY, M. & HALL, P. 1992 Small wavenumber Görtler vortices. *GJMAM* (submitted).

DENIER, J. P., HALL, P. & SEDDOUGHUI, S. O. 1990 On the receptivity problem for Görtler vortices: vortex motions induced by wall roughness. *ICASE Rep.*, 90-31 (referred to herein as DHS).

DENIER, J. P., HALL, P. & SEDDOUGUI, S. O. 1991 On the receptivity problem for Görtler vortices: vortex motions induced by wall roughness. *Phil. Trans. R. Soc. Lond.* A **335**, 51–85 (referred to herein as DHS).

HALL, P. 1982*a* Taylor–Görtler vortices in fully developed or boundary layer flows: linear theory. *J. Fluid Mech.* **124**, 475–494.

HALL, P. 1982*b* On the nonlinear evolution of Görtler vortices in growing boundary layers. *J. Inst. Maths Applics.* **29**, 173.

HALL, P. 1983 The linear development of Görtler vortices in growing boundary layers. *J. Fluid Mech.* **130**, 41–58.

HALL, P. 1984 On the instability of the unsteady boundary layer on a cylinder oscillating transversely in a viscous fluid. *J. Fluid Mech.* **146**, 347–368.

HALL, P. 1988 The nonlinear development of Görtler vortices in growing boundary layers. *J. Fluid Mech.* **193**, 247–266.

HALL, P. & HORSEMAN, N. 1991 The inviscid secondary instability of fully nonlinear longitudinal vortex structures in growing boundary layers. *J. Fluid Mech.* **232**, 357–375.

HALL, P. & LAKIN, W. D. 1988 The fully nonlinear development of Görtler vortices in growing boundary layers. *Proc. R. Soc. Lond.* A **415**, 421–444.

HALL, P. & SEDDOUGUI, S. O. 1989 On the onset of three-dimensionality and time-dependence in Görtler vortices. *J. Fluid Mech.* **204**, 405–420.

PRANDTL, L. 1935 *Aerodynamic Theory*. Springer.

RUBAN, A. I. 1990 Propagation of wave packets in the boundary layer on a curved surface. *Izv. Akad. Nauk. SSSR, Mekh., Zhudk. Gaza* **2**, 59–68.

SABRY, A. S. & LIU, J. T. C. 1991 Longitudinal vorticity elements in boundary layers. *J. Fluid Mech.* **231**, 615–664.

TIMOSHIN, S. N. 1991 Asymptotic analysis of the Görtler vortex spectrum. *Fluid Dyn.*, January 1991, 25.